Scientific Research Publishing

Materials Sciences and Applications, 2024, 15, 431-449
https://www.scirp.org/journal/msa
ISSN Online: 2153-1188
ISSN Print: 2153-117X

Geochemistry and Microstructure of Construction Materials from the Eastern Districts of N'Djamena Chad with a View to Their Stabilization in the Building and Pottery

Warabi Bebbata[1,2], Frédéric Pagore Djoda[1,3*], Madjihingam Ndjolba[1,4], Bertin Pagna Kagonbé[5], Raïdandi Danwé[1]

[1]Department of Civil Engineering, National Advanced School of Engineering, University of Maroua, Maroua, Cameroon
[2]Department of Civil Engineering and Architecture, Faculty of Engineering Sciences, University of Francophony (UNF), N'Djamena, Chad
[3]Laboratory of Mechanic and Material Processing (L2MP), Higher Teacher's Training for Technical College, University of Douala, Douala, Cameroun
[4]National Advanced School of Public Works, N'Djamena, Chad
[5]Local Materials Authority Promotion (MIPROMALO), Yaoundé, Cameroon
Email: frdjodap@gmail.com, *djodap@yahoo.fr

How to cite this paper: Bebbata, W., Djoda, F.P., Ndjolba, M., Kagonbé, B.P. and Danwé, R. (2024) Geochemistry and Microstructure of Construction Materials from the Eastern Districts of N'Djamena Chad with a View to Their Stabilization in the Building and Pottery. *Materials Sciences and Applications*, **15**, 431-449.
https://doi.org/10.4236/msa.2024.1510029

Received: August 24, 2024
Accepted: October 9, 2024
Published: October 12, 2024

Abstract

The early collapse of habitats in the spontaneous neighborhoods of the South-East of N'Djamena city pushed us to carry out investigations on the soil characteristics of the Ambatta 1 (Z1), Ambatta 2 (Z2), and Siguété (Z3) neighborhoods in this city. XRF (X-Ray Fluorescence), XRD (X-Ray Diffraction), FTIR (Fourier Transform InfraRed), SEM (Scanning Electron Microscopy), and ATG/DTA (Thermogravimetry Analysis/Differential Thermal Analysis) were conducted for microstructural and thermal identification. The geochemistry of the three soils studied revealed the presence of SiO_2 (49.03% - 73.80%), Al_2O_3 (08.35% - 17.34%), and Fe_2O_3 (03.79% - 10.90%) as major elements. The alkalines and alkaline earth elements include potassium K_2O (02.57% - 03.07%), magnesium MgO (0.47% - 01.21%), titanium TiO_2 (0.81% - 01.41%), sodium Na_2O (01.01% - 01.13%) and calcium CaO (01.28% - 03.28%). The fire loss of 09.90% on average remains low. XRD revealed the presence of quartz (~64.28%), feldspar (~07.14%), which are non-clay minerals, and clay minerals like kaolinite (~14.85%), illite (~07.14%) and some traces of smectite and amphibite on all three sites. These oxides were confirmed by FTIR analysis through peaks illustrating the vibrational movements specific to these oxides. SEM shows particles in the increasingly shaped, rounded, shiny sand grains. This is the presence of quartz. These quartz micro textures of abrasive surfaces

and topography with conchoidal fractures predict promising mechanical results. Smectite appears in wavy clusters, kaolinite in the form of shiny crystals, and illite materializes by the irregularity of the crystalline shape. These constituents are represented by the presence of their oxides specified by geochemistry. Thermally, the three samples overall retain more than 94% of their constituent on average for a temperature range reaching 950˚C, which predestines them for specific applications. Thus, this study aims to stabilize constructions using local materials after having mastered their constituents.

Keywords

N'Djamena East Soils, Physicochemical, Microstructural and Thermal Characterization

1. Introduction

The availability of sandy and clayey soils is global. The Sudano-Sahelian areas are not exempt because of their geographic and structural diversity and their ecosystems [1]. Managing the instability of said soils due to their structural variance remains a concern for users, especially for their stability [2]. The phenomena of absorption and desorption of water during the rainy seasons accelerate the degradation process of said spontaneous habitats built with local materials. The immediate consequences are direct cracks visible on buildings and also on road infrastructures [3]. Investigations were carried out to better understand the behavior of the soils of the Ambatta 1, Ambatta 2, and Siguété districts and to know whether they are clayey types [4] or not, silicate types or not based on their mineralogy and their physical properties [5]. This is generalized with the problem of determining the identity of the soils of the areas on the banks of the Logone [6]. This is because of the massive deterioration of spontaneous habitats in the new neighborhoods of towns in Sudano-Sahelian localities in general and the three sites mentioned above in particular. This is one of the reasons why researchers and public authorities are investing more and more in the control of said soils. The context of valorization of local resources in a structural and ceramic diversity [5] [7] [8] will not be too much. The objective of our work is to control and determine their constituents based on the identification of the different oxides that characterize them. Geochemical studies on these soils could allow the characterization of certain oxides, indicating precisely the variants of clayey soils and non-clayey soils. These coming from rivers winding through the study areas not only have an impact on socio-economic and environmental activities [9] but also on structural performance, which makes it possible to predict the geochemical formulation on certain sites. The essence of these oxides gives an idea of certain mechanical properties based on the chemical-mechanical bonds generated by these ores [10]. On the other hand, very sandy areas present fluidic and elastoplastic properties due to soil flow generated by torrential rains, having an impact on the modification of the intrinsic

constituents of said soils. However, certain neighboring areas in the northeast of the city of N'Djamena have clayey soils predisposed to the manufacture of ceramic objects [11] or their raw materials [12]. The sites of the Ambatta 1, Ambatta 2, and Siguété districts are also giving rise to new investigations based on chemical and microstructural analyses aimed at highlighting their constituents [13]-[16]. This is how geochemical analyses will be carried out to identify the oxides of the ores [17] that these soils could constitute. Then, the XRD will intervene to list the types of ores [18] and confirm the geochemistry results. The vibrational functions of the bonds that could generate the elements indexed by the XRD are highlighted by peaks specifying the types of bonds generated through the FTIR [19] [20].

Soil identification is also done from a morphological point of view. Stacks of platelets or clusters of crystals are analyzed by scanning electron microscopy [21]. Analyzes can be carried out to assess their ability to withstand and retain their essential constituents under the effects of temperature. The loss of mass as a function of temperature is characterized by thermogravimetric analysis [22]. The different transformation phases are determined by differential thermal analyses [23], which complement the TGA. All these analyses are there to effectively predict the behavior of said materials and their combination with other local substances to constitute composite materials for proven use. Especially since these floors are malleable and retractable, which suggests a viscoelastoplastic profile. This article aims to stabilize constructions using local materials based on the control of their constituents.

2. Materials and Methods

2.1. Location of Study Areas

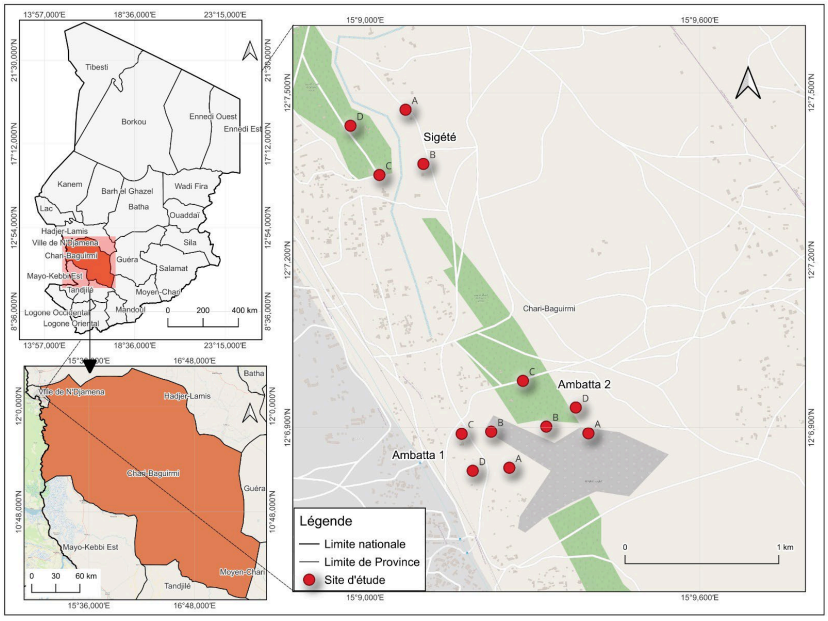

Figure 1. Below shows the three sites from which samples are taken.

Studies sites (Ambatta 1, Ambatta 2 and Siguété) are located in the South-East of N'Djamena Chad (Figure 1).

2.2. Hardware

The material that was the subject of all these analyses is essentially the soil powders taken from the Ambatta 1 (Z1), Ambatta 2 (Z2), and Siguété (Z3) sites, presented in Figure 2, to which must be added the different experimental devices in the laboratory. Several samples were taken from all the different site areas. This is why Z1, Z2, and Z3 samples are fully representative of the entire study area and take into account all the specific variations relating thereto. Densities (Kg/m^3) of Z1, Z2, and Z3 soils are 25.30, 24.52, and 25.1, respectively. The particle size distribution of these same soils is presented as follows: for Z1, 25% of clay, 40% of silt, and 35% of sand; for Z2, 56% of clay, 36% of silt, and 8% of sand and finally for Z3, 48% of clay, 34% of lemon and 18% of sand.

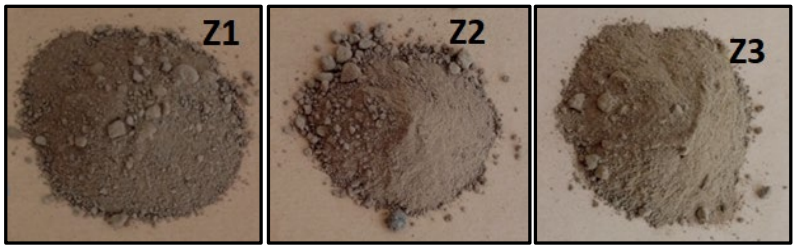

Figure 2. Samples Z1, Z2 and Z3.

2.3. Experimental methods and setup

This second part of the study aims to present the manipulation techniques and experimental protocols that made it possible to carry out all the analyses. Z1, Z2, and Z3 samples are representative of the study areas. Indeed, a Z1 sample represents the synthesis of several other samples from the same study locality. This is the same case for Z2 and Z3.

2.3.1. X-Ray Fluorescence (XRF) Geochemistry

The chemical composition was measured by X-ray fluorescence spectroscopy (XRF). The experiment was carried out using a Bruker S8 Tiger 4 kW spectrometer installed at the Cameroon cement plant (Cimencam of the Lafarge group), where 1 g of each sample was liquefied in 8 g of $Na_2B_4O_{710}H_2O$.

2.3.2. X-Ray Diffraction (XRD)

XRD is used here to verify the structural information of the three powder samples studied, Z1, Z2, and Z3.

The analysis is carried out using a Bruker diffractometer whose characteristics are Cu Kα1 anticathode with variation in wavelength at $\lambda = 1.5418$ Å, voltage V = 40 kV, and intensity I = 30 mA. The angle is used on $2^\circ < 2\theta < 70^\circ$ with steps of 0.02˚ and time-frequency in steps of 2 s, in the Bragg-Brentano θ/θ Configuration. The maximum intensities of the models used are both qualitative and semi-

quantitative [24] [25].

2.3.3. Fourier Transform Infrared Spectroscopy (FT-IR)

Infrared spectroscopy is used to identify bonds formed in mineral species based on vibrational frequencies. Each bond is made up of atoms or groups of atoms with their own vibrational frequencies. The experiment was carried out on a Bruker Alpha-P spectrometer (Thermo Electron) in absorbance mode. Then, the spectra were recorded in the spectral range (250 - 4000) cm^{-1} with a resolution of 4 cm^{-1}.

2.3.4. Thermal Analysis

TDA/TGA thermal analyses are used to detect and identify molecules by their mass measurement. Its principle lies in the gas phase separation of charged molecules (ions) according to their mass/charge ratio (m/z), then evaluating the heat released during exothermic and endothermic reactions. These analyses are carried out using a SetaramLABevo TG-DSC 1600˚C device, working under an Argon flow. Temperatures vary from room temperature up to 1200˚C in a ramp of 10 to 40˚C·min^{-1}. DSC data is obtained from the airflow of an Alumina crucible.

2.3.5. Scanning Electron Microscopy (SEM)

SEM is used on these ores to examine their morphology on a microscopic scale using a Philips model XL30 microscope (Liège, Belgium) equipped with electron beams accelerated under high voltage. Our samples are regularly placed on an appropriate support maintained in a vacuum of 5 × 10 cm^{-2} Pa.

3. Results and Interpretations

3.1. Geochemical Characterization of Studied Soils

Table 1. Geochemical composition of clay materials from the sites studied.

Oxides	Ambatta 1 (Z1)	Ambatta 2 (Z2)	Siguété (Z3)
SiO_2	73.80	49.03	64.44
Al_2O_3	8.35	17.34	12.46
Fe_2O_3	3.79	10.90	6.41
K_2O	3.07	2.57	2.97
MgO	0.47	1.21	0.60
TiO_2	0.81	1.41	1.03
P_2O_5	0.05	0.06	0.06
CaO	3.33	1.38	1.28
Na_2O	1.01	1.01	1.13
Mn_2O_3	0.07	0.14	0.11
LOI	5.26	14.95	9.51
SiO_2/Al_2O_3	8.84	2.83	5.17

The XRF chemical analyzes give the quantities of the different major chemical elements of the clay materials studied (**Table 1**). Observation of these results shows overall that samples studied are mainly made up of SiO_2, Al_2O_3, and Fe_2O_3 and a small proportion of MgO, MnO, CaO, Na_2O, K_2O, and P_2O_5.

Samples from the Ambatta 1 site contain 73.8% of SiO_2 and 8.35% of Al_2O_3. The Fe_2O_3 content is approximately 3.79%. The presence of alkalis and alkaline earth is remarkable: K_2O (3.07%), TiO_2 (0.81%), Na_2O (1.01%), CaO (3.33%) and MgO (0. 47%). Constituents such as manganese Mn_2O_3 at 0.07% and phosphorus P_2O_5 at 0.05%, although present, are negligible. The loss due to fire of these soils is, on average 8.84%. This value is relatively low.

The sample from the Ambatta 2 site also consists of SiO_2 (49.03%), Al_2O_3 (17.34%), and Fe_2O_3 (10.90%). The quantity of silica at 49.03% remains dominant over the other chemical elements on the site. The alkaline earth is similar to those of the first site: K_2O (2.57%), TiO_2 (1.41%), Na_2O (1.01%), CaO (1.38%), and MgO (1.21%) remain present. Other constituents, such as manganese (0.14%) and Phosphorus (0.06%), are insignificant. The loss due to fire is 2.83% and significantly lower than that of Ambatta 2 soils.

Analogous to the two previous sites, the results from the Siguété site present the same constituents with a few easy variations (**Table 1**). According to these results, we can affirm that the clay materials of these three sites are essentially composed of alumina silicate with an excess of quartz silica. These results are in agreement with the work of Kagonbé *et al*. [16], where the soils of Sudano-Sahelian zones with contrasting seasons are mainly composed of silica. The high quantities of alumina (Al_2O_3) observed in Z2 and Z3 samples show that these studied soils are made up of clay minerals such as kaolinite. This permanent presence of kaolinite alongside these minerals highlights this geochemical process called monosialization followed by bissialization [26].

The relatively high level of Fe_2O_3 comes from hematite identified by XRD and decomposition of clay minerals in the area. Alkalis and alkaline earths are relatively modest in these studied samples. The low values of CaO and MgO can be explained by the low content of carbonate minerals observed in most samples. The potassium and sodium oxide contents observed in the clay feedstock could likely be attributed to illite.

The positioning of the geochemical data of the studied clays in the triangular diagram (SiO_2-Al_2O_3-Fe_2O_3) showed that all samples were localized on the SiO_2-Al_2O_3 axis, toward the SiO_2 pole in line with high SiO_2/Al_2O_3 ratio (**Figure 3**). The ratio of SiO_2/Al_2O_3 is > 2.8 and ranges from 5.17 to 8.84, indicating excess silica content. The alumina and iron oxide values can be correlated with the presence of clay minerals [27]**.** The loss on fire is generally between 5.26% and 14.95 %. The highest rate of loss on fire is that of the Ambatta 2 locality. It follows that these soils would have undergone dehydroxylation reactions of clay minerals associated with the combustion of organic matter and the decomposition of the carbonate [28]. They also suggest, for the materials studied, the presence of other melting

minerals such as illite and smectite. The search for components capable of ensuring strong bonds must be explored to determine the thermomechanical properties of said materials.

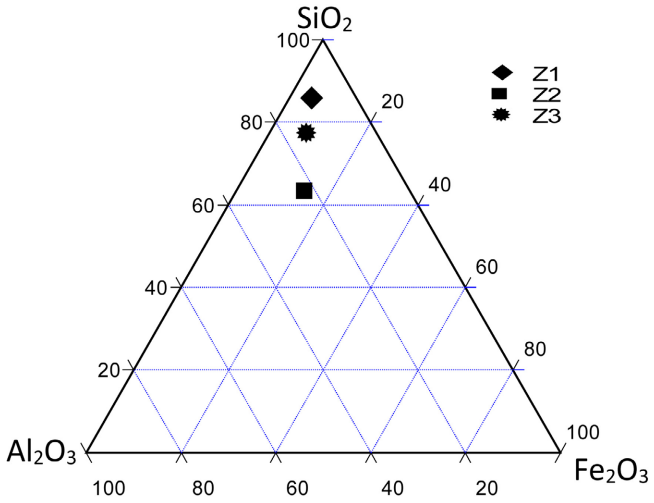

Figure 3. Geochemical composition of the studied soils in SiO_2-Al_2O_3-$Fe2O_3$ diagram.

3.2. Mineralogical Composition

3.2.1. X-Ray Diffraction

Figure 4 presents Z1, Z2, and Z3 samples diffractograms. These diffractograms show that the mineral procession of the studied soils consists of primary minerals (quartz, feldspars) and secondary minerals (kaolinite, smectites, illites, amphibole). The presence of illite is identified by the basal reflection around 9.55 Å, 10.05. Å, 10.08 Å matched with all these Z1, Z2 and Z3 samples. The amphibole is identifiable by the reflection at 8.52 Å. The kaolinite is found at the reflection at 7.26 Å, 7.08 Å, 7.00 Å (**Figure 3**). Quartz, which is the majority mineral, is identified by the reflections at 4.25 Å, 3.34 Å, 2.45 Å, 2.13 Å, 1.98 Å, 1.81 Å, 1.67 Å, 1.54 Å, 1.38 Å. The latest element is Feldspars at 4.03 Å, 3.78 Å, 3.55 Å, 3.24 Å. All ores obtained appear entirely at all three sites. These ores are almost the same. In addition, we note the notable presence of amphibole on the Ambatta 2 site. Its presence indicates a sedimentary deposit that has not yet transformed. Another type of ore appears plagioclase. It is a mineral from the feldspar family and tectosilicates with oblique cleavages. Its chemical composition varies from one crystal to another. We have, on the one hand, the albite with the chemical formula $NaAlSi_3O_8$ and, on the other hand, the anorthite $CaAl_2Si_2O_8$. Plagioclases are also called calcosodium feldspars. For comparison, the XRD of three samples shows basal reflections in the bumps form ranging from 7.00 to 15.00 Å, indicating the large amount of quartz compared to smectite, illite and kaolinite (**Figure 4**). The remaining reflection peaks are thin in size, which is characteristic of crystallites. This reflection for all of these samples indicates that the smectite has been characterized as a dioctahedral smectite; kaolinite at 7.26 Å is a mineral phase associated with smectite. In all samples, quartz (3.34 Å) and K-feldspars (2.24 - 4.01 Å)

coexist as accessory minerals. We deduce that quartz is the source of free silica in these soils, which is confirmed by the calculation of the SiO_2/Al_2O_3 ratio. This quartz content, with the addition of kaolinite is an asset in the formulation of compressed earth bricks.

The elongated shape of the characteristic peaks of these minerals shows that they are crystallized. The intensity of the quartz peaks proves that they are the majority throughout the mineralogical sphere. The variations observed in the mineralogy of these clay soils can be linked to the climatic conditions of the area, in particular the seasonal contrast, namely the long dry season and the short rainy season and explain their differential erodibility. This seasonal phenomenon is marked by the different phases of deposits observed both in the field. The presence of smectite associated with kaolinite suggests that the main crystallochemical processes involved are bissialitisation and monosiallitisation. Indeed, soils whose mineralogy is impacted by the presence of 2:1 type clay, such as smectite and kaolinite are sensitive to runoff and variable erosion as soon as they are saturated with water. This physical character will have an impact on the mechanical properties of materials from said soils, especially their resilience to the presence of water.

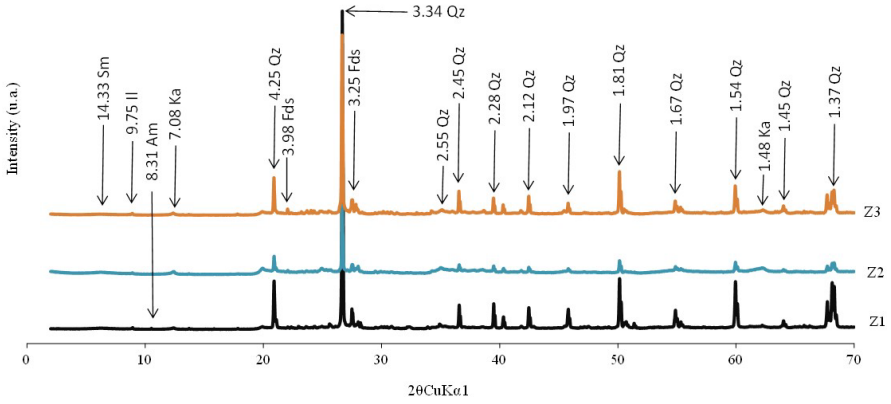

Figure 4. X-ray diffraction patterns of Z1_Z2_Z3 clay samples.

A comparative analysis is carried out with similar work in localities around the Lake Chad basin. Table 2 brings out the quintessence.

Table 2. Comparison with some ores around Lake Chad basin areas.

Characteristics	Current study	Ndjolba *et al.* 2024 [11]	Tsozué *et al.* 2022 [29]	Kagonbé *et al.* 2021 [16]	Nzeukou *et al.* 2021 [30]	Temga *et al.* 2013 [6]
Location	Eastern of N'Djamena	N'Djamena Southern	Maroua Dale	Garoua Dale	Logone Dale	Yagoua Lowland
Mineralogy	Smectite, illite, kaolinite, quartz, feldspar, amphibole	Smectite, illite, kaolinite, quartz, feldspar	Smectite, illite, kaolinite, quartz, feldspar, hematite	Smectite, illite, kaolinite, quartz, feldspar, hematite	Smectite, illite, kaolinite, quartz, feldspar, amphibole, hematite	Smectite, illite, kaolinite, quartz, feldspar

Continued

Geochemical	Sum of exchangeable bases (me/100 g)	Low	Moderate	Moderate	Moderate	Moderate
Physical properties	Bulk density [24.2 - 25.3]	Moderate	Low	//	Moderate	Low
	Weight loss [5.0 - 11.5]	Moderate	Low	High	//	//
Particle size distribution (%)	Clay: (<0.002 mm) [25.0 - 56.0]	High	High	High	Less	Medium
	Silt: (0.002 - 0.02 mm) [34.0 - 40.0]	High	Less	Less	Less	Less
	Sand: (0.02 - 2 mm) [8.0 - 35.0]	Less	High	High	High	Less
	Gravel: (>2 mm) 0.0	//	//	//	Less	Less
Atterberg limits (%)	Liquid limit (WL) [41.6 - 77.7]	Medium	Medium	High	Medium	High
	Plastic limit (WP) [25.6 - 41.2]	Medium	High	High	Medium	High
	Plastic index (IP) [16.0 - 36.8]	High	High	High	Medium	High

Relatively high silica contents specify very plastic sedimentary clays (Reeves *et al*., 2006), while the relative alumina (Al_2O_3) contents confirm the presence of smectites.

3.2.2. FTIR Analysis

Infrared spectroscopy is used here in addition to XRD. It is an excellent means of detecting organic compounds and mineral structures. The recording interval of our samples goes from 400 to 4000 cm^{-1} and presents vibrational and deformation bands specific to the minerals found.

The infrared spectrum of the Z1 sample (**Figure 5**) made it possible to highlight the assignments of the OH groups and those of other related networks. Generally, interval bands 4000 - 3500 cm^{-1} are those of hydroxyl groups. The elongation vibration bands ranging from 3697 cm^{-1} to 3649 cm^{-1}, characteristic of clay, are attributed to the inter-layer hydroxyl groups of kaolinite. Their intensities and positions are generally sensitive to the intercalation of organic molecules. The characteristic band at 3620 cm^{-1} is specifically attributed to external hydroxyls with sheets insensitive to intercalations. The presence of these significant vibrational bands supposes that this kaolinite extracted from this clayey soil has a disordered structure [31]. The weak bands ranging from 1900 to 2300 cm^{-1} belong to the amine groups, which represent impurities for this work. The band at 1633 cm^{-1} is specific to the vibration of the OH groups of the hydration water of the soil sample studied; this same band shows the presence of smectite. Between 1000 and 900 cm^{-1} the angular vibration bands are those of Si-O of Kaolinite. Likewise, the Al-OH and Al-O-Si deformation vibration bands appear from 911.23 cm^{-1} [32]-[34]. The presence of quartz is identified at 775.82 cm^{-1}. Around 550 to 400 cm^{-1}, the Si-O-M bonds (M designate the metals Al, Mg and Fe located in an octahedral position) are recorded.

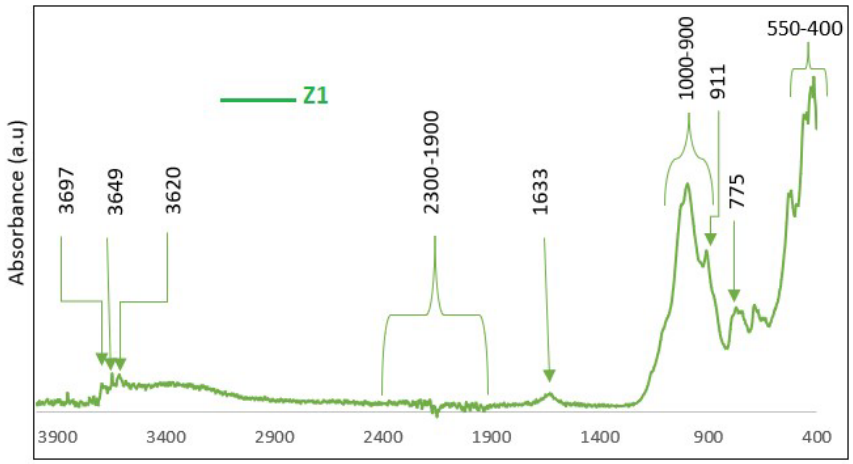

Figure 5. Infrared spectra of a Z1 sample.

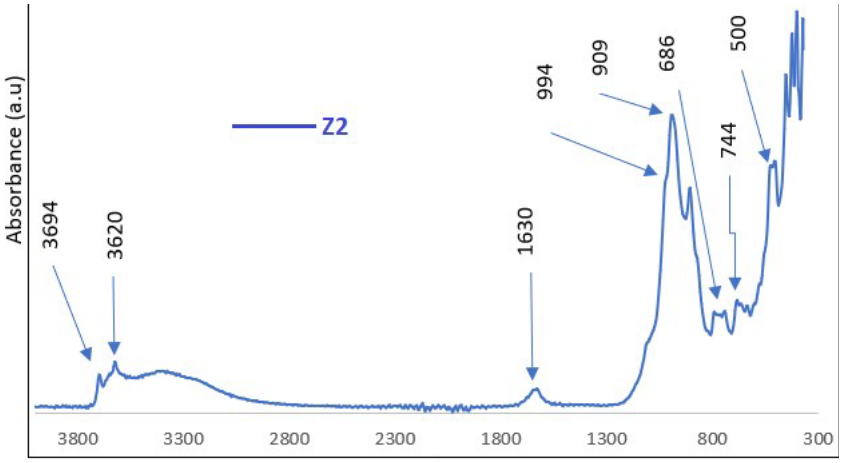

Figure 6. Infrared spectra of a Z2 sample.

Some similarities are recorded between the IR spectra of Z2 and Z1 samples (Figure 6). As for Z1, hydroxyl bands at 3694.43 and 3620.46 cm^{-1} are characteristic of kaolinite. The weak band at 1630.12 cm^{-1} materializes the aluminosilicate in the amorphous phase. The vibration bands at 994.19 cm^{-1} and 909.07 cm^{-1} are those of Si-O Kaolinite. They also correspond to deformation vibrations of Al-OH-Al and Al-O-Si, which will disappear to give way to broadband with a sharp peak at 994.19 cm^{-1}, belonging to the Si-O-Si bonds of the kaolinite. This modification would be due to the formation of an amorphous structure, as already mentioned during XRD analyses (Figure 4). The weak peaks around 686.60 cm^{-1} simultaneously justify the presence of quartz and kaolinite in the SiO_4 group. These vibrations correspond to Al-O bonds. The peak band at 744.96 cm^{-1} is those of the C-O bonds of calcite. Like Z1, in the interval 550 - 400 cm^{-1}, it is the Si-O-M bonds (M designate Al, Mg, and Fe metals located in an octahedral position) that are recorded. Bands at 2170.98 and 2095.12 cm^{-1} are respectively attributed to the (δ

+ ν) Al_2-OH and $2\nu Al_2$-OH modes of the aluminous phyllosilicate's family, including smectite, kaolinite, and muscovite [35]. Although indicated by XRD, quartz and feldspars absorb very little radiation in the visible or near-infrared range, hence their few apparent peaks.

Z1 and Z2 sample bands study allows us to deduce the composition and identification of the peaks observed on Z3 (Figure 7) because of the similar bands observed. This is how the two peaks of the bands at 3695.78 and 3620.14 cm^{-1} are attributable to the vibrations of the OH groups of the kaolinite already specified previously. The interpretation is identical to that of site Z1 except that here, the area appears more stable. The peaks located at the interval 3300 to 3500 cm^{-1} specify gibbsite bands in these soils [36]-[38]. The band at 1635.08 cm^{-1} belongs to the group of aluminosilicates in the amorphous phase. The rest of the bands, ranging from 1000 to 400 cm^{-1} are specified in samples Z1 and Z2.

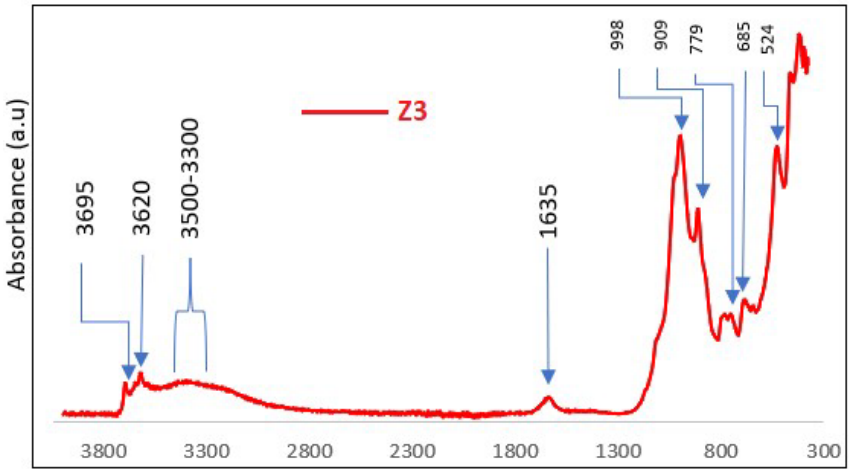

Figure 7. Infrared spectra of sample Z3.

We note on all three sites a similarity in the bands corresponding to the minerals observed. The Ambatta 2 site seems closer to Siguété in terms of constituents; this is because of the direct depression of Siguété towards Ambatta 2 before arrival towards Ambatta 1. That is why the Ambatta 1 soil is full of all the deposits of "impurities" characterized by constituents belonging to the amine group and other non-minerals.

3.2.3. Morphological Analysis

The three samples are submitted as taken from the study sites to avoid the amorphization of these ores and the preservation of the material structure. The morphological configuration of Z1, Z2, and Z3 soil samples from the Ambatta 1, Ambatta 2, and Siguété sites, respectively, are presented in Figure 8. We can give these different structures two interpretation types.

The particles that appear on the surface as shiny sand grains are mostly rounded (Figure 8_Z1_Z2_Z3): it is the presence of quartz. The micro textures of the

quartz grains on the surface of these samples can exhibit both mechanical and chemical characteristics (**Figure 8**_Z1). The shapes presented in their micro textures have inhomogeneous surfaces with a topography of conchoidal fractures (**Figure 8**_Z2), provided with multiform concavities (**Figure 8**_Z1_Z2). These shapes are adapted to particle rearrangement during the consolidation of the material structure [39]. The superposition of small, more or less wavy clusters in platelets marks the presence of smectite already indicated by the XRD of Z2, while the planar crystalline forms are attributable to kaolinite. The small shiny bulbs observed on all three samples mark the presence of kaolinite on all three sites. The very varied texture with cavities and porous openings, associated with scattered aggregates of circular and somewhat complex shape, is characteristic of the presence of kaolinite particles. This morphology of the kaolinite particles is visible throughout **Figure 8**. The presence of crystals stacked on top of each other in clusters with irregular grain sizes is characteristic of illite. This is also noticeable in all three samples.

The presence of oxides obtained by geochemistry is found in SEM images by the multitude of clusters scattered across all three samples with a high content of SiO_2, Al_2O_3, and FeO. These elements are characteristic of crystallized kaolinite because of their irregular morphology [40]. The bright crystals formed in agglomeration illustrate carbonate formations, which are specific to quartz. The superposition of wavy clusters reveals the presence of smectite (**Figure 8**_Z2).

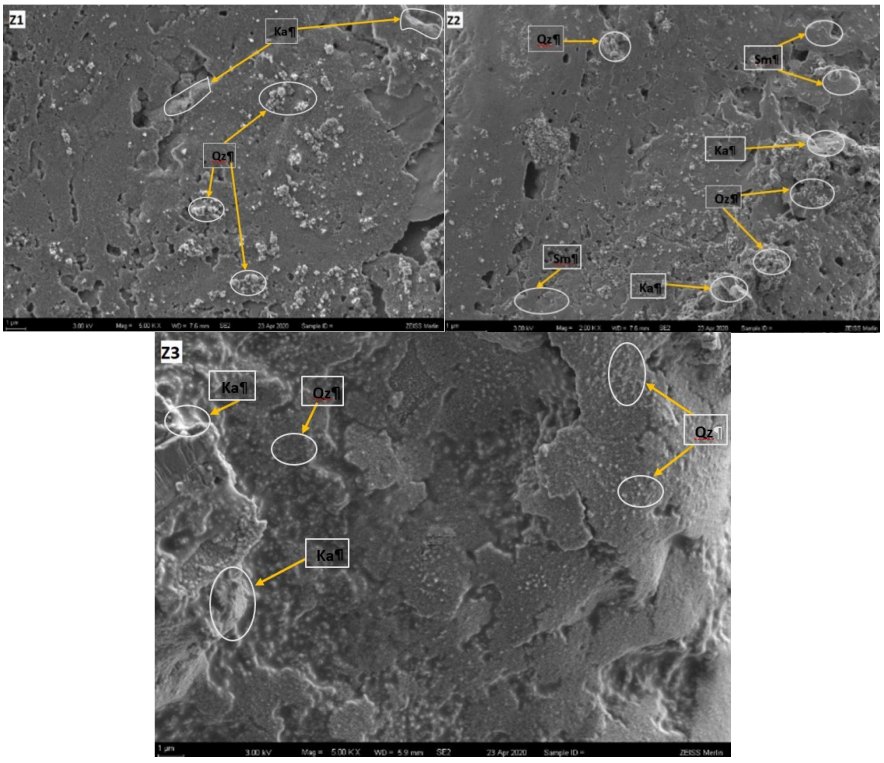

Figure 8. Morphological images of Z1, Z2 and Z3 samples.

The morphology of the balls observed is generally kaolinite (**Figure 8**_Z1_Z2).

The clusters are mostly stacked on top of each other, accompanied by crystals formed on the surface. The irregularity of this granular topography is characteristic of the illite, which is grafted onto all three samples.

3.2.4. Thermal Analysis

Figures 9, **10**, and **11** are TGA curves giving the mass losses of Z1, Z2, and Z3 samples. The analysis of these curves leaves similar characteristics. These mass losses recorded on the TGA curves can be presented in three phases. The first difference in height on these curves is attributable to the water loss for each sample. The second drop corresponds to the decomposition of organic matter and hydroxides. The last drop in level materializes mineralogical transformations.

The Z1 Sample presents a mass loss of 1.88%, followed by Z3 with 1.98%, and finally, Z2 for a value of 4.14%. This means that Z1 and Z3 accumulate fewer ambient water molecules than Z2. This mass loss is less than 2% for a temperature oscillating around 250˚C for Z1 and Z3, while for Z2 we are at more than 4% mass loss for a temperature hovering around 200˚C. For the three samples, the second elevations generally show that these materials withstand a large amount of heat. The temperatures range from around 200˚C to 500˚C for Z2 and from 250˚C to 500˚C for Z1 and Z3. The resulting mass losses are 2.83% for Z1, 2.91% for Z3 and 4.95% for Z2. The third difference in height corresponds to the phase where the mass loss is the lowest for the three samples: 1.31% for Z1, 1.46% for Z3 and 2.43% for Z2. It appears that Z1 retains more than 98% of its constituents in the first temperature range located between 0˚C and 250˚C, between 250˚C and 500˚C it retains even more than 95.2% and from 500˚C to 950˚C the TGA curve tends asymptotically while retaining almost 94% of its mineralogical constituents. Z2 retains more than 95% of its constituents at the first temperature range between 0˚C and 200˚C, then between 200˚C and 540˚C it retains more than 90%, and finally, its TGA curve tends asymptotically to more than 88% for a temperature range of up to 950˚C. Sample Z3 has a thermal behavior similar to Z1. Z3 retains more than 93.5% for a temperature reaching 1000˚C.

Each of the phases observed on the three TGA curves involves endo and exothermal transformations on the joint ATD curves (**Figure 9**, **10**, **11**). This is how the differential thermal analyses (DTA) present variations in the heat flux for each of the three samples. In **Figure 9**, **10**, and **11**, three endothermic peaks are visible for samples Z1 and Z3 and two for sample Z2. See also exothermic peaks.

The mass loss recorded between 0˚C and 200˚C for the three samples Z1, Z2, and Z3, corresponding to the hygroscopic departure of water within the illite sheets [41], materialized specifically by the first endothermic peaks on the TDA curves. The second, more perceptible endothermic peaks on these three curves appear between 480˚C and 540˚C. This temperature range corresponds to the hydroxylation of kaolinite and later to its transformation into meta kaolinite. It is also at this temperature range that we witness the release of hydroxide formed during the crosslinking of the bonds made up of oxide networks on the ores responsible for the presence of kaolinite, illite, and quartz. [13] [23] [42].

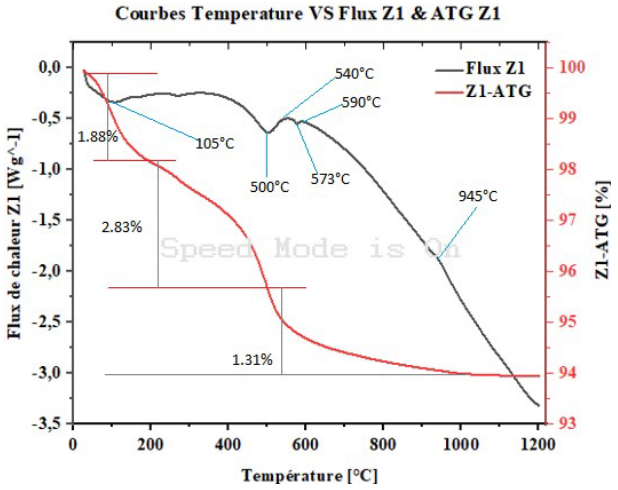

Figure 9. TG and DTG curves of clay soils from Ambatta 1 (Z1).

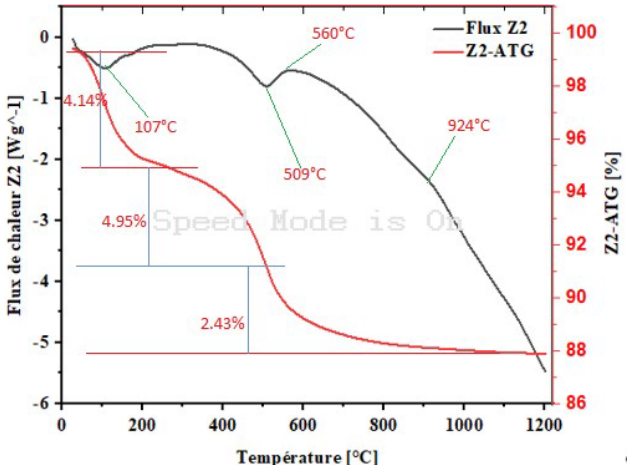

Figure 10. TG and DTG curves of clay soils from Ambatta 2 (Z2).

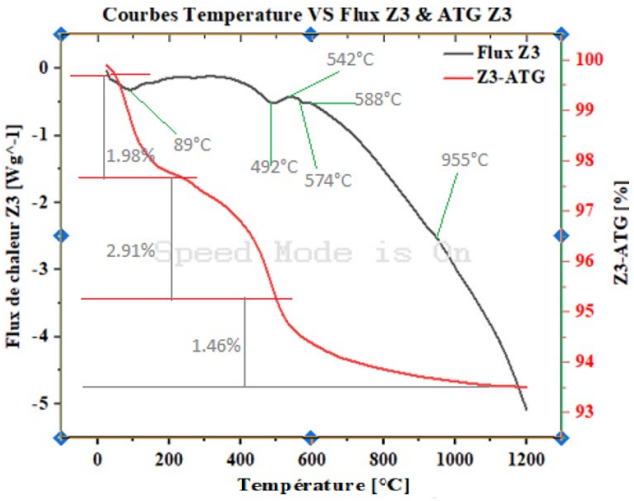

Figure 11. TG and DTG curves of clay soils from Siguete (Z3).

The rise in the curve (slight exothermic peak) around 480˚C for Z1, around 490˚C

for Z2, and 510˚C for Z3 marks the hydroxylation phase of illite and smectite for these three samples. The second rise, marked by a slight bump around 620˚C for Z1 and 650˚C for Z3 (but non-existent for Z2), characterizes the beginning of the transformations relating to the structural reorganization of oxides of kaolinite, magnesium, illite, and many others.

The third exothermic peak in the form of barely perceptible bumps is observable on all three samples on the DTA curves. The temperatures corresponding to this phase vary from 950˚C to 1000˚C. These bumps mark the beginning of the organic matter and hydroxyl decompositions, the transformation of quartz, and the loss of carbonates. It should be said that all three study areas could withstand high temperatures.

Indeed, it should be noted that before 900˚C, several phenomena are observable. Endothermic peaks recorded at 500˚C for Z1, at 509˚C for Z2, and then 492˚C for Z3 are attributable to the dihydroxylation of the OH groups of kaoline on the one hand and to their transformation into metakaolinite on the other. It should be added that the dihydroxylation temperature of the kaolinite of the three samples is lower than 600˚C, which means that these types of kaolinites are disordered [43]. It could contain stacking faults on their crystallographic axis [44]. In addition, the endothermic peaks around 573˚C for Z1 and 574˚C for Z3 reflect the transformation of quartz α into β. The exothermic phenomena at 945˚C for Z1, 924˚C for Z2, and 955˚C for Z3 are due to the metakaolinite structural reorganization.

4. Conclusion

The mineralogical constituents of the soils in the Ambatta 1, Ambatta 2, and Siguété localities were highlighted by specific analyses. Geochemical, microstructural, and thermal tests were carried out. Geochemistry on these soils revealed the presence of SiO_2 (49.03% to 73.80%), Al_2O_3 (8.35% to 17.34%), Fe_2O_3 (3.79% to 10.90%) as major elements and others in small proportions such as K_2O (2.57% to 3.07%), TiO_2 (0.81% to 1.41%), Na_2O (1.01% to 1.13%), CaO (1.28% to 3.33%), and MgO (0.47% to 1.21%) which are alkaline and alkaline-earthy. The loss on ignition varying from 5.26% to 14.95% is in line with the thermal test values. Indeed, TGA analyses show a mass loss that varies from 6.02% to 11.52%. The TDA analysis shows that these soils begin to deteriorate under the action of heat from 900˚C. This proves that these areas are predisposed to withstand high-temperature fluctuations. XRD revealed two types of ores. Non-clay ores such as quartz (64.28%) and feldspar (7.14%), then clay ores such as kaolinite (14.28%), illite (7.14%) and smectite (7.14%) are essential constituents of these soils. Infrared also highlighted peaks that materialize vibratory movements of the oxides presented by XRD. The diversity of shapes and visual texture obtained by SEM elucidate the presence of nuanced clay particles in porous cavities, to which must be added inter-aggregates whose shapes, sometimes circular, sometimes hexagonal, characterize kaolinite. The compilation of other grains into clusters of crystals characterizes

illite and many other oxides whose presence has already been specified by other analyses. The bright crystals spread across all three SEM images are characteristic of quartz and are responsible for the presence of several oxides. These oxides all have free atoms capable of forming future strong bonds in the presence of an additional additive from an appropriate matrix. Thus, early collapses are elucidated, and palliatives are recommended.

Conflicts of Interest

The authors declare no conflicts of interest regarding the publication of this paper.

References

[1] Ndong, A.T., Ndiaye, O., Sagna, M.B., *et al*. (2015) Caractérisation de la végétation ligneuse sahélienne du Sénégal: cas du Ferlo. *International Journal of Biological and Chemical Sciences*, **9**, 2582-2594. https://doi.org/10.4314/ijbcs.v9i6.6

[2] Agbelele, K.J., Houehanou, E.C., P'Kla, A., Dossou, I.A. and Aristide, H.C. (2023) Stabilization of Clay Soil for the Durability of Structures: Case Study of the Soils of the Locality of Zalimé, Commune of Zogbodomey in the Republic of Benin. *Open Journal of Civil Engineering*, **13**, 103-112. https://doi.org/10.4236/ojce.2023.131007

[3] Amer, A.A., Mattheus, F.A.G. and Ghazi, A.A. (2006) Geology, Classification, and Distribution of Expansive Soils and Rocks: A Case Study from the Arabian Gulf Expansive Soils. CRC Press.

[4] Kissou, R., Gnankambary, Z., Nacro, H.B. and Sedogo, M.P. (2018) Classification locale et utilisation des sols en zone sahélienne au Burkina Faso. *International Journal of Biological and Chemical Sciences*, **12**, 610-617. https://doi.org/10.4314/ijbcs.v12i1.46

[5] He, I.L., Atheba, G.P., Allou, N.B., Drogui, P., Khakani, M.A.E. and Gbassi, G.K. (2023) Physic, Chemical and Mineralogical Characterizations of Clays Used in the Making of Traditional Ceramics in the City of Katiola, Côte d'Ivoire. *Journal of Minerals and Materials Characterization and Engineering*, **11**, 81-91. https://doi.org/10.4236/jmmce.2023.114008

[6] Temga, J.P., Mazzù, A., Nguetnkam, J.P., Palazzini, D., Ndjouenkeu, R. and Vitali, F. (2013) Valorisation of Crude Earth as Sustainable Building Material: A Case of International Cooperation in the Logone Valley (Chad-Cameroon). *International Journal of Sustainable Engineering*, **7**, 222-234. https://doi.org/10.1080/19397038.2013.807886

[7] Nshimiyimana, P., Fagel, N., Messan, A., Wetshondo, D.O. and Courard, L. (2020) Physico-chemical and Mineralogical Characterization of Clay Materials Suitable for Production of Stabilized Compressed Earth Blocks. *Construction and Building Materials*, **241**, Article ID: 118097. https://doi.org/10.1016/j.conbuildmat.2020.118097

[8] Bentahar, Y., Draoui, K., Hurel, C., Ajouyed, O., Khairoun, S. and Marmier, N. (2019) Physico-Chemical Characterization and Valorization of Swelling and Non-Swelling Moroccan Clays in Basic Dye Removal from Aqueous Solutions. *Journal of African Earth Sciences*, **154**, 80-88. https://doi.org/10.1016/j.jafrearsci.2019.03.017

[9] Kagonbé, B.P., Nafissa, B., Djeutchou, C., Hamdja, A.N., Djoda, P., Loabé, A.P., *et al*. (2024) Gravel and River Sand Mining Activities in Maroua (Far-North Region, Cameroon): Environmental and Socioeconomic Aspects. *Archives of Agriculture and Environmental Science*, **9**, 126-133. https://doi.org/10.26832/24566632.2024.0901018

[10] Zhang, C., Bai, Q., Han, P., Wang, L., Wang, X. and Wang, F. (2023) Strength Weakening and Its Micromechanism in Water-Rock Interaction, a Short Review in Laboratory Tests. *International Journal of Coal Science & Technology*, **10**, Article No. 10. https://doi.org/10.1007/s40789-023-00569-6

[11] Madjihingam, N., Pagore, D., Mache, J.R., Warabi, B., Kagonbe, B.P. and Kouotou, P.M. (2024) Clay Materials for Ceramics Application from N'Djamena in the Chad Republic: Mineralogical, Physicochemical and Microstructural Characterization. *Journal of Materials Science and Chemical Engineering*, **12**, 31-48. https://doi.org/10.4236/msce.2024.122003

[12] Asante-Kyei, K., Addae, A. and Aflo, A. (2023) Developing Recipe from Local Ceramic Raw Materials for Making Crucibles in Ghana. *Journal of Minerals and Materials Characterization and Engineering*, **11**, 92-113. https://doi.org/10.4236/jmmce.2023.114009

[13] Munvuyi, D., Ousmane, M.S. and Bougouma, M. (2022) Physicochemical and Mineralogical Characterization of Clays from the Tcheriba Zone in the Boucle of Mouhoun Region (Burkina Faso). *Journal of Materials and Environmental Science*, **13**, 755-767. http://www.jmaterenvironsci.com.

[14] Basga, S.D., Temga, J.P., Tsozué, D., Danbé, N. and Nguetnkam, J.P. (2018) Morphological, Mineralogical and Geochemical Features of Topomorphic Vertisols Used for Sorghum Production in North Cameroon. *Eurasian Journal of Soil Science* (*EJSS*), **7**, 346-354. https://doi.org/10.18393/ejss.460841

[15] Mache, J.R., Signing, P., Mbey, J.A., Razafitianamaharavo, A., Njopwouo, D. and Fagel, N. (2015) Mineralogical and Physico-Chemical Characteristics of Cameroonian Smectitic Clays after Treatment with Weakly Sulfuric Acid. *Clay Minerals*, **50**, 649-661. https://doi.org/10.1180/claymin.2015.050.5.08

[16] Kagonbé, B.P., Tsozué, D., Nzeukou, A.N. and Ngos III, S. (2021) Mineralogical, Geochemical and Physico-Chemical Characterization of Clay Raw Materials from Three Clay Deposits in Northern Cameroon. *Journal of Geoscience and Environment Protection*, **9**, 86-99. https://doi.org/10.4236/gep.2021.96005

[17] Nguetnkam, J.P., Villiéras, F., Kamga, R., Ekodeck, G.E. and Yvon, J. (2014) Mineralogy and Geochemical Behaviour during Weathering of Greenstone Belt under Tropical Dry Conditions in the Extreme North Cameroon (Central Africa). *Geochemistry*, **74**, 185-193. https://doi.org/10.1016/j.chemer.2013.06.007

[18] Madejová, J. and Komadel, P. (2001) Baseline Studies of the Clay Minerals Society Source Clays: Infrared Methods. *Clays and Clay Minerals*, **49**, 410-432. https://doi.org/10.1346/ccmn.2001.0490508

[19] Moussout, H., Ahlafi, H., Aazza, M., Chfaira, R. and Mounir, C. (2020) Interfacial Electrochemical Properties of Natural Moroccan Ghassoul (Stevensite) Clay in Aqueous Suspension. *Heliyon*, **6**, e03634. https://doi.org/10.1016/j.heliyon.2020.e03634

[20] Linker, R., Kenny, A., Shaviv, A., Singher, L. and Shmulevich, I. (2004) Fourier Transform Infrared—Attenuated Total Reflection Nitrate Determination of Soil Pastes Using Principal Component Regression, Partial Least Squares, and Cross-Correlation. *Applied Spectroscopy*, **58**, 516-520. https://doi.org/10.1366/000370204774103327

[21] Cases, J., Liétard, O., Yvon, J. and Delon, J. (1982) Étude des propriétés cristallochimiques, morphologiques, superficielles de kaolinites désordonnées. *Bulletin de Minéralogie*, **105**, 439-455. https://doi.org/10.3406/bulmi.1982.7566

[22] Jozanikohan, G., Sahabi, F., Norouzi, G.H. and Memarian, H. (2015) Thermal Analysis: A Complementary Method to Study the Shurijeh Clay Minerals. *International Journal of Mining& Geo-Engineering*, **49**, 33-45.

[23] Wang, Q., Odlyha, M. and Cohen, N.S. (2000) Thermal Analyses of Selected Soil Samples from the Tombs at the Tianma-Qucun Site, Shanxi, China. *Thermochimica Acta*, **365**, 189-195. https://doi.org/10.1016/s0040-6031(00)00723-1

[24] Cook, H.E., Johnson, P.D., Matti, J.C. and Zemmels, I. (1975) Methods of Sample Preparation and X-Ray Diffraction Data Analysis, X-Ray Mineralogy Laboratory, Deep Sea Drilling Project, University of California, Riverside. In: Kaneps, A.G., *et al*., Eds., *Initial Reports of the Deep Sea Drilling Project*, U.S. Government Printing Office, 999-1007. https://doi.org/10.2973/dsdp.proc.28.app4.1975

[25] Fagel, N., Boski, T., Likhoshway, L. and Oberhaensli, H. (2003) Late Quaternary Clay Mineral Record in Central Lake Baikal (Academician Ridge, Siberia). *Palaeogeography, Palaeoclimatology, Palaeoecology*, **193**, 159-179. https://doi.org/10.1016/s0031-0182(02)00633-8

[26] Nguetnkam, J.P., Kamga, R., Villiéras, F., Ekodeck, G.E. and Yvon, J. (2008) Altération différentielle du granite en zone tropicale. Exemple de deux séquences étudiées au Cameroun (Afrique centrale). *Comptes Rendus. Géoscience*, **340**, 451-461. https://doi.org/10.1016/j.crte.2008.02.002

[27] Tsozué, D., Nzeugang, A.N., Mache, J.R., Loweh, S. and Fagel, N. (2017) Mineralogical, Physico-Chemical and Technological Characterization of Clays from Maroua (Far-North, Cameroon) for Use in Ceramic Bricks Production. *Journal of Building Engineering*, **11**, 17-24. https://doi.org/10.1016/j.jobe.2017.03.008

[28] Temga, J.P., Nguetnkam, J.P., Balo Madi, A., Basga, S.D. and Bitom, D.L. (2015) Morphological, Physico Chemical, Mineralogical and Geochemical Properties of Vertisols Used in Bricks Production in the Logone Valley (Cameroon, Central Africa). *International Research Journal of Geology and Mining*, **5**, 20-30. http://dx.doi.org/10.14303/irjgm.2015.108

[29] Tsozué, D., Nzeukou, A.N., Kagonbé, B.P., Madi, A.B., Mache, J.R., Bitom, D.L., *et al*. (2022) Genesis and Assessment of Clay Materials Suitability for Earthenware Production in Northern Cameroon. *Arabian Journal of Geosciences*, **15**, Article No. 1376. https://doi.org/10.1007/s12517-022-10603-7

[30] Nzeukou Nzeugang, A., Tsozué, D., Kagonbé Pagna, B., Balo Madi, A., Fankam Deumeni, A., Ngos, S., *et al*. (2021) Clayey Soils from Boulgou (North Cameroon): Geotechnical, Mineralogical, Chemical Characteristics and Properties of Their Fired Products. *SN Applied Sciences*, **3**, Article No. 551. https://doi.org/10.1007/s42452-021-04541-4

[31] Khireddine, O., Berredjem, Y., Hailaimia, F., Nouacer, S., Djellaibi, R., Bensid, N., *et al*. (2016) Removal of *Para*-Nitrophenol by Adsorption on Intercalated Natural Clay. *Sensor Letters*, **14**, 258-265. https://doi.org/10.1166/sl.2016.3647

[32] Farmer V.C. (1974) The Infrared Spectra of Minerals. Mineralogical Society. https://doi.org/10.1180/mono-4

[33] Frost, R.L. and Vassallo, A.M. (1996) The Dehydroxylation of the Kaolinite Clay Minerals Using Infrared Emission Spectroscopy. *Clays and Clay Minerals*, **44**, 635-651. https://doi.org/10.1346/ccmn.1996.0440506

[34] Wilson, M.J. (1994) Clay Mineralogy: Spectroscopic and Chemical Determinative Methods. Chapman & Hall. https://doi.org/10.1007/978-94-011-0727-3

[35] Madejová, J., Pentrák, M., Pálková, H. and Komadel, P. (2009) Near-Infrared Spectroscopy: A Powerful Tool in Studies of Acid-Treated Clay Minerals. *Vibrational Spectroscopy*, **49**, 211-218. https://doi.org/10.1016/j.vibspec.2008.08.001

[36] Balan, E., Lazzeri, M., Morin, G. and Mauri, F. (2006) First-Principles Study of the Oh-Stretching Modes of Gibbsite. *American Mineralogist*, **91**, 115-119.

https://doi.org/10.2138/am.2006.1922

[37] Bardy, M., Fritsch, E., Derenne, S., Allard, T., do Nascimento, N.R. and Bueno, G.T. (2008) Micromorphology and Spectroscopic Characteristics of Organic Matter in Waterlogged Podzols of the Upper Amazon Basin. *Geoderma*, **145**, 222-230. https://doi.org/10.1016/j.geoderma.2008.03.008

[38] Janik, L.J., Forrester, S.T. and Rawson, A. (2009) The Prediction of Soil Chemical and Physical Properties from Mid-Infrared Spectroscopy and Combined Partial Least-Squares Regression and Neural Networks (PLS-NN) Analysis. *Chemometrics and Intelligent Laboratory Systems*, **97**, 179-188. https://doi.org/10.1016/j.chemolab.2009.04.005

[39] Ekoa Bessa, A.Z., Armstrong-Altrin, J.S., Fuh, G.C., Bineli Betsi, T., Kelepile, T. and Ndjigui, P. (2021) Mineralogy and Geochemistry of the Ngaoundaba Crater Lake Sediments, Northern Cameroon: Implications for Provenance and Trace Metals Status. *Acta Geochimica*, **40**, 718-738. https://doi.org/10.1007/s11631-021-00463-5

[40] Hattab, M., Bouziri-Adrouche, S. and Fleureau, J. (2010) Évolution de la microtexture d'une matrice kaolinitique sur chemin triaxial axisymétrique. *Canadian Geotechnical Journal*, **47**, 34-48. https://doi.org/10.1139/t09-098

[41] Milošević, M., Logar, M. and Djordjević, B. (2020) Mineralogical Analysis of a Clay Body from Zlakusa, Serbia, Used in the Manufacture of Traditional Pottery. *Clay Minerals*, **55**, 142-149. https://doi.org/10.1180/clm.2020.20

[42] Mielenz, R.C., Schieltz, N.C. and King, M.E. (1953) Thermogravimetric Analysis of Clay and Clay-Like Minerals. *Clays and clay minerals* (*National Conference on Clays and Clay Minerals*), **2**, 285-314. https://doi.org/10.1346/ccmn.1953.0020124

[43] Michot, A. (2008) Caractéristiques thermophysiques de matériaux à base d'argile: Évolution avec des traitements thermiques jusqu'à 1400˚C. Master's Thesis, Université de Limoges.

[44] Letellier, M.C. (1986) Récupération et dosage des phases argileuses d'un sable de gisement. Ph.D. Thesis, University of Toulouse.